ORIGINAL RESEARCH ARTICLE

# Microstructure Engineering During Wire-Arc Additive Manufacturing of High-Strength Martensitic Steels

M. TAYLOR, J. WANG, Y.H. MOZUMDER, S.W. WILLIAMS, F. SCENINI, P.B. PRANGNELL, and E.J. PICKERING

Martensitic steel components produced using wire-arc additive manufacturing (WAAM) can contain coarse, highly textured columnar prior austenite grain (PAG) structures in the as-built state, which may exacerbate cracking issues during building and are difficult to remove with conventional post-build heat treatments. Here, we demonstrate that fine PAG structures can be achieved in WAAM'd martensitic steel by using a sufficiently low interpass temperature and ensuring a large enough heat-affected zone (HAZ) depth relative to the deposited layer height. It was found that controlling these two conditions during the building of 300M steel ensured that each layer of steel deposited was repeatedly cycled between austenite and martensite, refining the PAGs since they were in the HAZs of subsequent layers. The interpass temperature and HAZ depth required for 300M were found using dilatometry followed by electron backscatter diffraction (EBSD) mapping and validated through the microstructural characterization of three 300M WAAM walls built with different interpass temperatures and HAZ overlaps. EBSD characterization revealed that, when austenitised, 300M exhibited a memory effect that was followed by recrystallisation without applied external deformation. Importantly, since the grain refinement was achieved through austenite-martensite cycling, it is highly likely that the principles exploited here could be applied to achieve similar grain refinement in other martensitic steels.

https://doi.org/10.1007/s11661-025-07988-x
© The Author(s) 2025

## I. INTRODUCTION

WHEN compared with traditional ingot casting and forging, wire-arc additive manufacturing (WAAM) could be a more sustainable option for manufacturing large metallic components with complex geometries, as it enables the production of near-net-shape components that require significantly less machining. This is especially important when manufacturing high strength steels, which are difficult to machine. WAAM offers several advantages for the manufacturing of the large high-spec martensitic steel components often used in aerospace when compared with other additive manufacturing techniques. This is in part due the fast deposition rate of WAAM (many kgs/hr), but the unrestricted part size and the low number of safety-critical lack of fusion or pore type defects.[1–3] However, martensitic steel WAAM builds can suffer from issues including residual stresses and quench cracking. Moreover, many as-built martensitic steel builds found in the literature[4–6] have anisotropic microstructures when compared with their conventionally manufactured equivalent, as they often contain large grain sizes resulting from millimetre-scale columnar prior austenite grains (PAG) and significant compositional microsegregation of alloying elements. For aerospace steels such as 300M, the properties associated with these grain structures do not comply with aerospace standards (AMS 6419, AMS 6257 or ASTM E112) and would require lengthy cyclic austenitisation treatments to refine,[7,8] as a single post-build austenitisation treatments may not always provide sufficient refinement.[9] Furthermore, large PAGs in 300M have been associated with poor mechanical properties including weld cracks,[10] a reduction in notch-toughness, and the segregation of impurities to these boundaries, particularly in low sulfur steels.[11–13]

To date, a few authors[4,14–16] have performed microstructural characterization and/or mechanical testing on 300M walls built using WAAM. It is relevant for

M. TAYLOR, Y.H. MOZUMDER, F. SCENINI, P.B. PRANGNELL, and E.J. PICKERING are with the Department of Materials, and Henry Royce Institute, The University of Manchester, Manchester, M13 9PL, UK. Contact e-mail: mark.taylor-5@manchester.ac.uk J. WANG and S.W. WILLIAMS are with the Welding and Additive Manufacturing Centre, Cranfield University, Cranfield MK43 0AL, UK.
Manuscript submitted June 16, 2025; accepted September 16, 2025.



Published online: 27 September 2025

this study to mention that interpass (or interlayer) temperature in 300M has been studied before by Xiong *et al.*[15] using cold metal transfer (CMT) WAAM. With this process, they concluded that 200 °C was the optimal interpass temperature due to a lack of micropores and better 'surface waviness'. Lower interpass temperatures were deemed unsuitable due to cleavage fractures during tensile testing. However, it is important to note that all mechanical testing in this study was performed whilst the steel was in the as-built condition, rather than the final quench and tempered condition required by a component. Furthermore, PAG sizes across the build could not be measured due to the small area electron back scatter diffraction (EBSD) mapped. A later study by Xiong *et al.*[16] did investigate the tensile properties of a post-heat treatment CMT WAAM build, however the PAG size was not measured.

Whilst previous studies have significantly advanced our understanding of 300M microstructures in additive manufacturing, there are areas where interpretations are debatable in the view of the current authors. For instance, mechanical testing has often been performed only in the as-built condition,[14,15,17,18] without considering the requirements for developing final product tempers. This makes it challenging to build upon previous works. For example, as-deposited 300M microstructures retain compositional microsegregation, which forms as a result of solute partitioning and dendritic growth from the melt pool.[19,20] By employing optical microscopy, we also believe that authors[14,21–23] might have misinterpreted compositionally enriched regions as grain boundaries, where the compositional difference (most likely Cr enrichment) causes them to etch lighter than the surrounding microstructure. However, PAG boundaries do not necessarily match up with the dendritic or cellular segregation pattern revealed by etching or by energy dispersive spectroscopy (EDS), and in some examples, they may exist on different length scales entirely, as demonstrated by Taylor *et al.*,[9] by comparing in situ EBSD austenite grain measurements with EDS analysis from the same area. Additionally, the meso-scale heterogeneous nature and evolution of the microstructure across multiple deposited layers is rarely included in published work due to challenges associated with the limited field width imaged using electron microscopy and microanalysis techniques. As a consequence, large columnar microstructures may be missed. We believe that the large-area EBSD PAG reconstruction by Jun *et al.*[4] demonstrates how a 300M WAAM deposit can sometimes contain a complex pattern of repeating bands of columnar and equiaxed grains created by overlapping HAZs, a long-range grain structure variation that would not have been revealed by selecting a random single field of view with conventional EBSD mapping. To the author's present knowledge, there has yet to be a systematic study of the microstructural evolution of 300M as it is repeatedly reheated by overlapping HAZs during WAAM, or how altering this HAZ overlap effects the microstructural heterogeneity across the build. By understanding this and the conditions needed to produce a desirable 300M microstructure, a set of materials-based thermal conditions could be defined to inform the criteria the welding parameters of any specific WAAM set up must achieve.

In many martensitic steels including 300M, grain refinement may be achieved through the application of multiple austenitisation treatments[7,24]—the overall PAG size reducing further with each cycle from martensite to austenite and back again. The present paper investigates whether a grain-refining cyclic austenitisation treatment may be implemented during the WAAM process itself, eliminating large columnar PAG structures in the as-built condition. The concept relies on the following two suppositions: (i) that if the interpass temperature used is below the steels materials martensite start temperature ($M_s$), then last deposited bead should be martensitic before the next pass is deposited; (ii) that if the HAZ of the next layer deposited is large enough, it may austenitise previous layers, effectively subjecting them to a cyclic heat treatment. Here, the concept is demonstrated building with 300M, a medium carbon low-alloy high strength steel currently used in aerospace applications.

The present work also aimed to identify the minimum reheat temperature, minimum interpass temperature and minimum number of austenitisation cycles required to achieve grain refinement in 300M. From these, the necessary heat-affected zone (HAZ) depth relative to the layer height was determined. Dilatometry and electron backscatter diffraction (EBSD) were employed as tools to obtain these parameters, enabling the definition of a processing window for successful grain refinement based solely on the material's thermal response.

## II. EXPERIMENTAL METHODS

### A. *Overview*

The experiments are presented as three consecutive, interrelated studies, each designed based on the findings of the previous one. The first study aimed to demonstrate that a grain refinement mechanism based on using the correct interpass temperature works in practice during WAAM. For this, the microstructures of two 300M builds were compared, one built using a low interpass temperature that was below the $M_s$ of 300M, and one built with a high interpass temperature that was above the $M_s$. The second study aimed to determine the precise thermal conditions needed to achieve grain refinement in 300M during thermal cycling (*i.e.,* the thermal conditions that must be met in the HAZ created during building). This was achieved through a heat treatment matrix that assessed different peak temperatures, interpass temperatures, and numbers of heating cycles, whilst using typical WAAM heating and cooling rates. This matrix was performed using a dilatometer and subsequent EBSD analysis of the samples. The third study characterized a build with a different heat input to demonstrate the effect HAZ size, or specifically the depth of austenitisation, has on refinement.

The compositions of all 300M used in this study were measured by optical emission spectroscopy (OEM) after building, these are shown in Table I and the WAAM processing parameters for each build in used in these experiments are collated in Table II. The compositional differences are minimal and they are not expected to affect the findings of the work.

### B. *Builds for Study 1*

To study the effect of interpass temperatures during 300M WAAM (Study 1), two WAAM walls (multi-pass in the normal direction) were produced by Cranfield University with a plasma tungsten arc (PTA) process on mild steel substrates. One was allowed to cool to an interpass temperature of 100 °C (low interpass build) in between each pass, and one which was built continuously with as high an interpass temperature as practically possible (high interpass temperature). Interpass temperature was measured using six K-type thermocouples inserted into holes drilled into the baseplate in the positions shown in Figures 1(a), (b) and using a long-wavelength FLIR A655sc infrared (IR) camera positioned above the deposit. After building, cross-sections used for microstructural characterization were extracted from above the central two thermocouples as illustrated in Figure 1(c). The thermocouples used a data acquisition frequency of 50 Hz and enabled the shape of the temperature profile underneath the heat source to be measured as illustrated in Figures 1(d) and (e) using centrally positioned thermocouples from the low and high interpass builds, respectively. The IR camera was calibrated using thermocouples, with the emissivity determined to be 0.21. Figures 1 (f), (g) display a frame from the end of the 3$^{rd}$ layer deposition for the low and high interpass builds, respectively. It illustrates how IR was used to evaluate the thermal accumulation. For the low interpass temperature build, the next layer was not deposited until the temperature measured on the IR camera, thermocouples and an additional thermometer operated manually reached at least 100 °C. The dimensions of the builds were approximately 17.5 × 15 × 270 mm$^3$ and 22 × 12 × 270 mm$^3$ (height × width × length) respectively, all processing parameters were otherwise kept identical between builds (see Table II). The microstructures of either build's cross-section were characterized using optical microscopy, a large-area EBSD montage with PAG reconstructions, EDS, secondary electron (SE) and backscatter electron (BSE) imaging (see details below).

### C. *Heat Treatments for Study 2*

To understand the microstructural evolution during reheating in the HAZ of 300M, and thus determine the conditions that lead to a refined grain structure during thermal cycling (Study 2), 4 × 10 × 2 mm$^3$ (diameter × length × hole diameter) hollow dilatometry samples were machined from the high interpass temperature build in the as-built condition, the long axis of the sample parallel to the long axis of the wall. This build was selected as it was found to have a bulk microstructure consisting of coarse columnar PAGs, similar to those found in the as-deposited top layer of any build, as will be discussed later. A TA instruments Dil805 A/D/T dilatometer with fused silica pushrods and S-type thermocouples was used to replicate typical WAAM heating temperature profiles measured by a thermocouple positioned in the centre of the baseplate of the low interpass temperature build [shown in Figure 1(e)]. Heating was performed under vacuum to prevent decarburization and cooling under an Ar atmosphere to achieve the desired cooling rates. The initial pass from this temperature profile was systematically modified as shown in Figure 2 to determine the following behaviour of 300M:

- The minimum peak temperature reached within the HAZ, with WAAM equivalent heating rates, that is required to achieve grain refinement. This was investigated using single heating cycles, as shown in Figure 2(a). Peak temperatures of 870 °C (standard 300M austenitisation treatment temperature), 950 °C, 1000 °C, 1050 °C and 1100 °C were used.
- The minimum interpass temperature required between deposition and reheating, investigated using the temperature profiles shown in Figure 2(b). These tests consisted of two heating cycles and interpass temperatures of 300 °C, 250 °C, 200 °C, 150 °C, and 100 °C between them. They were conducted with prior knowledge of the peak temperature experiments. Therefore, an initial peak temperature of 870 °C was used for the first cycle since it was known this would reproduce the original columnar austenite grains via a memory effect, as discussed later. The peak temperature used for the second heat was 1000 °C, as this was known to lead to some grain refinement after a single heat.
- The minimum number of heating cycles required for substantial grain refinement. Between 1 and 4 cycles were performed, a 1000 °C peak temperature and a 100 °C interpass was used for each. The temperature profiles used are shown in Figure 2(c).

**Table I. Composition of the 300M Used in this Work Measured Using OES by Element Materials Technology PLC**

| Samples | C | Cr | Mn | Mo | Ni | P | S | Si | V |
|---|---|---|---|---|---|---|---|---|---|
| Study 1-2 | 0.42 | 0.85 | 0.80 | 0.38 | 1.76 | 0.006 | 0.008 | 1.66 | 0.08 |
| Study 3 | 0.41 | 0.81 | 0.74 | 0.41 | 1.92 | 0.006 | < 0.003 | 1.68 | 0.08 |

Table II. WAAM Parameters Used to Build Each Wall Investigated in this Work

| WAAM Parameters | Wire Feeding Speed (m $min^{-1}$) | Torch Travel Speed (mm $s^{-1}$) | Deposition Current (A) | Gas Flowrate (L $min^{-1}$) | Shielding Condition | Interpass Temperature |
|---|---|---|---|---|---|---|
| Study 1 Low Interpass Single Bead Width | 2.35 | 3.3 | 210 | 0.8 | Ar global shielding with oxygen level < 500 ppm | ~ 100 °C |
| Study 1 + 2 High Interpass Single Bead Width | 2.35 | 3.3 | 210 | 0.8 | Ar global shielding with oxygen level < 500 ppm | Continuous deposition |
| Study 3 CWMIG Oscillated | 7 | 16.8 | 225 | 25 | Specshield 8 pct $CO_2$ in Ar Local shielding | ~ 150 °C |

Throughout the test matrix, the heating rate (200 °C $s^{-1}$) and cooling profile (see Figure 2) were kept constant to replicate the conditions experienced in the austenitised region of a WAAM HAZ. After heat treatment, the samples were sectioned in half to form doughnut-shaped cross-sections, and an EBSD montage map was recorded from each. The PAG structures were reconstructed to determine whether an individual heat treatment had successfully eliminated the original coarse columnar PAG structures. These tests aimed to elucidate which conditions within a HAZ would lead to a refined grain structure, and which would not.

In addition to the above, one extra dilatometry sample was heated to 870 °C at a constant heating rate of 100 °C $s^{-1}$ and a cooling rate of the same, without any hold at temperature. This test was designed to produce a clean and consistent dilatometry curve for calculating the volume fraction of martensite formed during cooling. Such a curve could not be obtained using the WAAM temperature profiles, as the thermocouple data ends just below 100 °C, and the change in cooling rate used to bring the samples to room temperature affects the measurement of the martensite finish temperature ($M_f$).

### D. *Builds for Study 3*

To study the effect of changing HAZ size (Study 3) a 50 × 25 × 130 $mm^3$ (height × width × length) multi-pass 300M wall was built by Additure with a cold wire metal inert gas (CWMIG) process and an oscillated build strategy. Further process parameters can be found in Table II. Based on the findings of studies 1 and 2, the wall was built with a 150 °C interpass temperature, measured in between layers using a pyrometer at the hottest end of the wall (where each layer deposition finished). Compared with the PTA walls, the CWMIG process here produced very different thermal gradients below the heat source, leading to different re-austenitisation depths below the melt pool. A wall cross-section was prepared for characterization using optical microscopy with polarized light (see details below). This allowed Study 3 to assess how variations in HAZ size—specifically, the depth of re-austenitisation—affect grain refinement. Crucially, the insights gained from Studies 1 and 2 enabled a forensic analysis of the HAZ, where specific microstructural features could be directly linked to corresponding thermal conditions.

### E. *Characterization Methods*

All the walls analyzed were sectioned transversely in their ND-TD plane through the centre of the walls length as shown in Figure 1(c). Slices 5 mm in thickness were ground and then polished to a 0.04 $\mu$m OPS finish. Dilatometry cross-sections were mounted in conductive Bakelite and polished similarly. All BSE imaging, EBSD and EDS were performed with the samples in this condition. The samples were then etched in a 2 pct nital solution, optical microscopy and SE imaging was then performed with the samples in this condition.

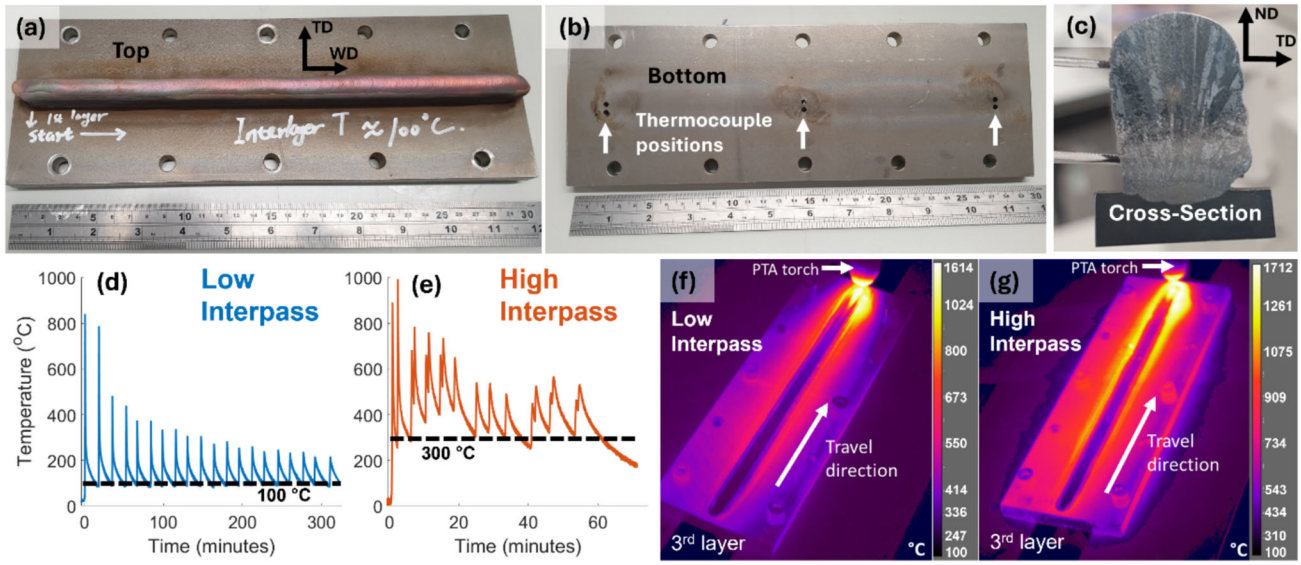


Fig. 1—(*a*) A top-down view of the low interpass temperature wall with (*b*) a view of the bottom of the baseplate with thermocouple holes highlighted by white arrows. (*c*) An etched cross-section cut from the high interpass wall. All walls were sectioned and imaged from this orientation. (*d*) The temperature profile recorded by a thermocouple during the low interpass temperature build. (*e*) The temperature profile recorded by a thermocouple during the high interpass temperature build. (*f*), (*g*) IR camera frames after finishing the 3rd layer of the low and high interpass temperature builds, respectively.

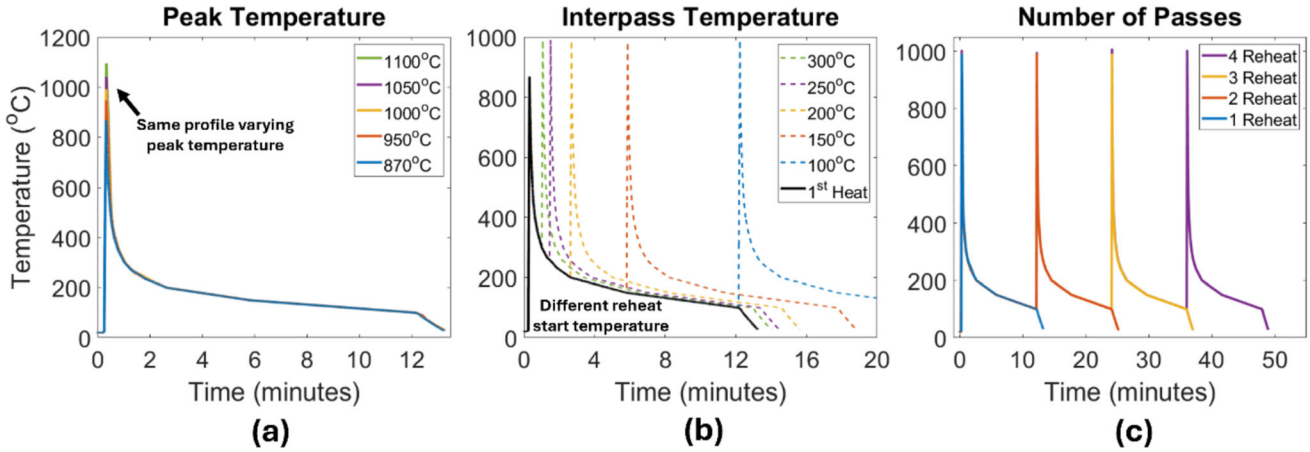


Fig. 2—Temperature profiles used for the dilatometry tests in study 2. (*a*) Peak temperatures were varied between 950 °C, 1000 °C, 1050 °C, 870 °C and 1100 °C. (*b*) Interpass temperatures between 1st and 2nd (dashed lines) heats were varied between 300 °C, 250 °C, 200 °C, 150 °C and 100 °C. (*c*) Between 1 and 4 heating cycles were investigated, with constant WAAM-replicated heating and cooling profiles.

Optical microscopy was performed on the builds using a Zeiss AxioImager M2m with an automated stage. Entire build cross-sections were imaged with a raster pattern and the individual images stitched together using Zeiss Zen software to produce an optical map of the sample. This was then repeated using polarized light. An FEI Magellan 400 SEM was used for secondary SE imaging with an accelerating voltage of 20 kV and a current of 0.4 nA. EBSD, BSE imaging and EDS were performed in a ThermoScientific Apreo SEM. For EBSD, 20 kV, a current of 51 nA and a 70° tilt were used with an Oxford Instruments Symmetry 2 detector. Maps were montaged and stitched using AZtec 6.1 SP2 software, and PAGs reconstructed using the AZtec Crystal 3.0 parent grain reconstruction tool with the Nishiama-Wassermann orientation relationship. The low interpass temperature build was mapped using a step size of 1.6 $\mu$m, the step size was then reduced to 0.11 $\mu$m when mapping a magnified region. For the high interpass temperature build, a 2 $\mu$m step size and 0.6 ms exposure time were used, whilst the step size was reduced for to 1 $\mu$m for the dilatometry samples. PAG reconstruction parameters were optimized for the individual maps, in all cases non-indexed pixels were filled in before reconstruction. For BSE and EDS, 15 kV and a current of 13 nA were used with an Oxford Instruments

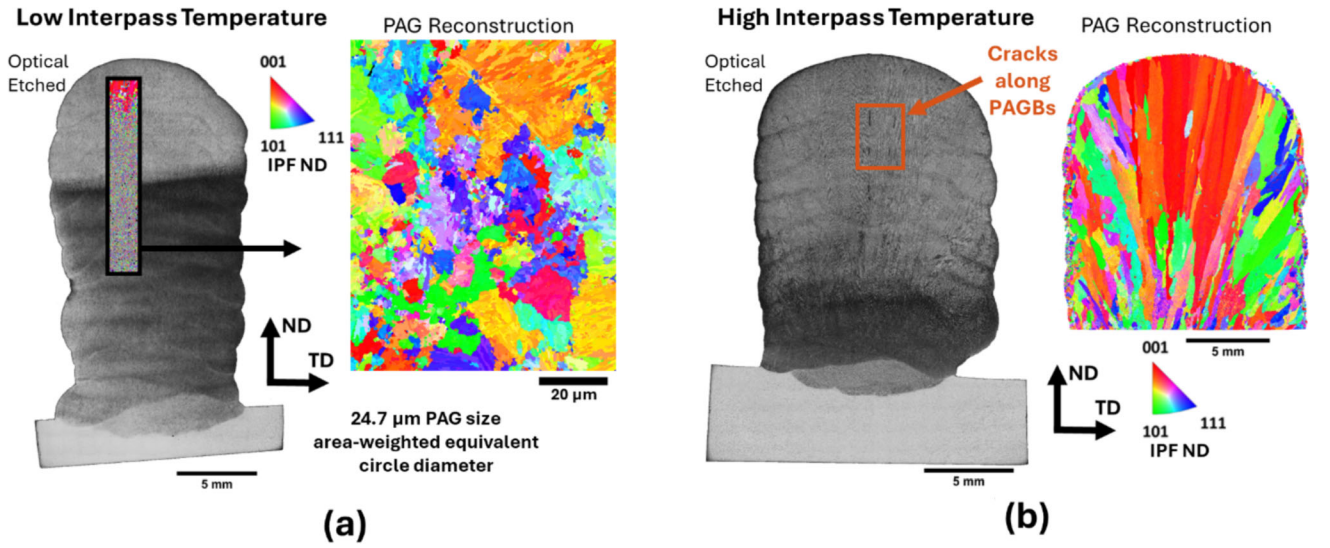


Fig. 3—(*a*) Montage optical map of the low interpass temperature build after etching. The PAG reconstruction of the montage EBSD map performed prior etching is overlaid on the image. An enlarged area of the PAG reconstruction is shown to the right with the average PAG diameter measured from bulk of the material (ignoring the unrefined columnar grains from the final layer) recorded below. (*b*) Montage optical map of the high interpass temperature build after etching, an EBSD PAG reconstruction of the entire build is displayed beside it. An area containing cracks is highlighted by the orange box. A magnified image of this area can be found in Fig. 5(a).

Ultim Max 170 detector. The carbon signal was not analyzed since it is well known to be inaccurate when using EDS.

## III. RESULTS

### A. *Study 1: The Effect of Interpass Temperature on PAG Structure*

Study 1 aimed to demonstrate the effect of changing the interpass temperature on the as-built prior austenite grain structure. Figures 1(d) through (g) display thermocouple data and IR camera frames and from the Study 1 low and high interpass temperature builds. The low interpass temperature build always maintained an interpass temperature of close to 100 °C, whilst the high interpass build remained at approximately 300 °C or above. It was assumed that the temperature inside the wall did not differ significantly from these values, since the walls were small and the values were based on both multiple thermocouple readings from inside the baseplate and IR camera data from the wall surface. The interpass temperature for the high interpass build was less consistent as it was allowed to cool intermittently to prevent overheating and material dripping over the sides. Optical maps showing whole build cross-sections are displayed in Figure 3 alongside EBSD PAG reconstructions of selected regions. Only a strip of the low interpass build was EBSD mapped in 3(a) owing to the small grain size necessitating the use of a small step size, creating time and computer memory restrictions. The entire high interpass build cross-section could be EBSD mapped using a larger step size due to its coarse PAG structure, and it is displayed in 3(b). A light etching region at the top of both builds can be seen in the optical micrographs. These are areas that cooled from austenite (high temperature above $A_{c3}$) after the last pass and formed martensite (they were not then subsequently thermally cycled below $A_{c3}$, which induces darker etching tempered microstructures[4]). The light etching region was much larger in the high interpass temperature build than in the low interpass build. EBSD PAG reconstructions revealed that the low interpass build contained a very fine PAG size (25 $\mu$m equivalent circle diameter) in all but the very final layer, which contained large columnar PAGs. The high interpass build consisted of very large columnar PAGs running continuously up through multiple deposited layers in the build. The central columnar grains were strongly textured with the ⟨100⟩ PAG axis aligned near to the normal (build) direction and presumably the direction of heat flow, as is commonly found in additively manufactured steels.[4,9,25] Additionally, the high interpass temperature build contained multiple cracks running parallel to the build and travel directions. EBSD confirmed that these cracks ran along PAG boundaries (PAGB), the largest is highlighted in the optical image in Figure 3(b).

SE micrographs of the light and dark etching regions of the low interpass temperature build are provided in Figures 4(a), (b). These images show that the microstructure of the top (light etching in optical) consisted of untempered martensite, whilst the bottom (dark etching) consisted of heavily tempered martensite (carbides have spheroidised). In comparison, the bottom (dark etching) regions of the high interpass build consisted of a mixture of bainite and martensite, whilst the top (light etching) contained untempered martensite interspersed with a few lower bainite sheaves.

The cracks found in the Study 1 high interpass temperature build [shown in Fig. 3 (b)] are magnified in Figures 5(a), and (b) illustrates that these cracks follow PAG boundaries. A region above one of the cracks is

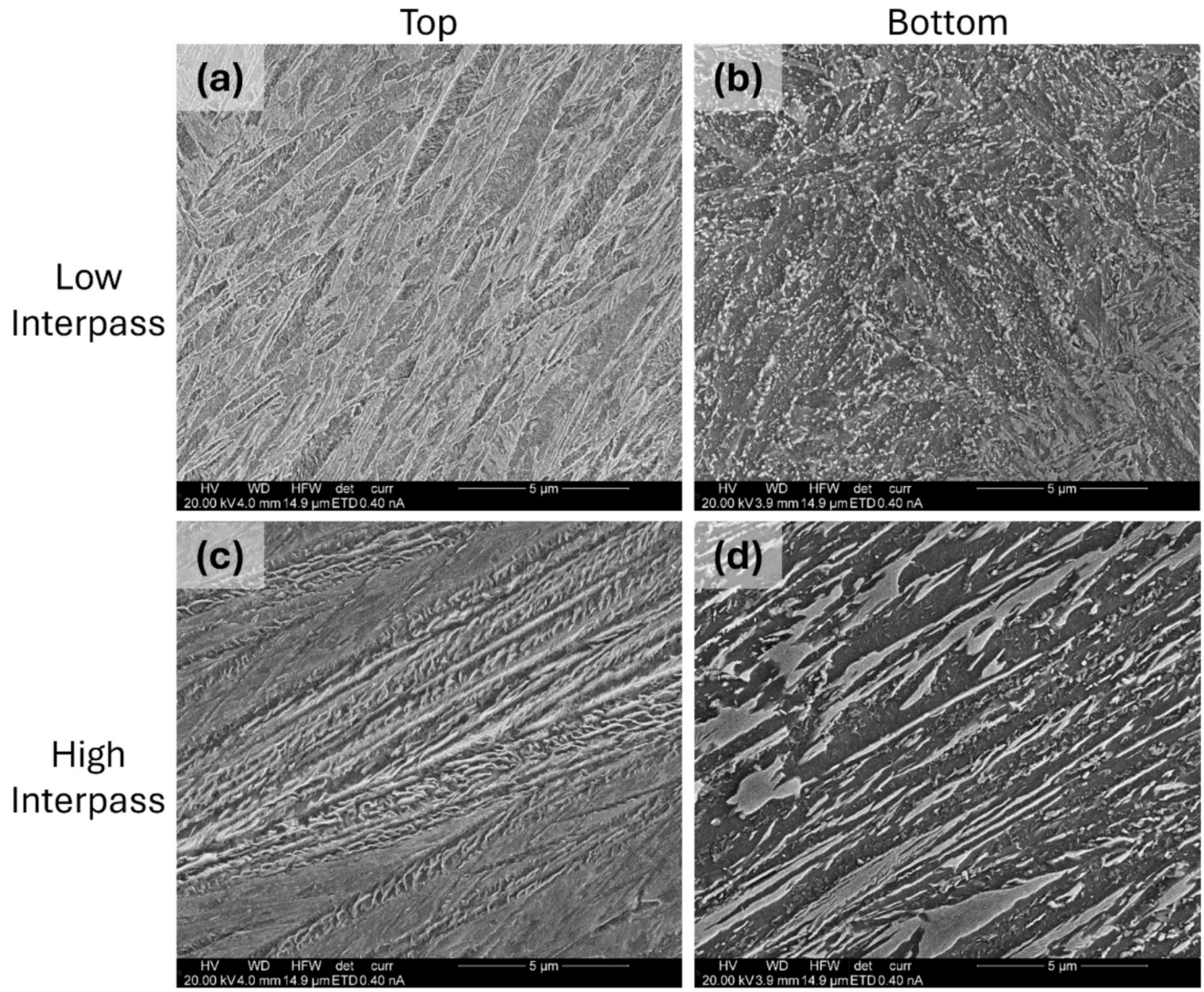


Fig. 4—SE images of the Study 1 build microstructures in an etched condition. (*a*) Untempered martensite in the top of the low interpass build. (*b*) Heavily tempered martensite from the middle-bottom of the low interpass build. (*c*) Lower bainite and untempered martensite from the top of the high interpass build. (*d*) Bainite from the middle-bottom of the high interpass build.

imaged using BSE imaging in Figure 5(c). The Si K$\alpha$ intensity EDS map in Figure 5(d) demonstrates that the crack follows an enriched interdendritic region, in addition to following a PAG boundary. Si was used to highlight this microsegregation as it gave the best contrast – other element maps for could have been used as all major alloying elements in 300M partition to interdendritic regions. Note that the spacing of the enriched interdendritic regions, which appear lighter in Figure 5(c) BSE map, is much finer than the size of the columnar PAGs [compare light etching regions in (a) to PAGs in (b)]. This means that interdendritic regions do not necessarily always coincide with PAG boundaries. S and Mn EDS intensity maps (e–f) reveal the presence of MnS particles along the PAG boundaries. Additionally, Table I shows that this build contained a higher wt pct of S than subsequent builds, where S content was below the sensitivity level of the OES measurement used.

### B. *Study 2: Finding the Conditions for PAG Refinement During Thermal Cycling*

The results of Study 1 above clearly demonstrated that control of the interpass temperature has an influence on austenite grain refinement during WAAM deposition. Study 2 aimed to define the thermal processing window required for grain refinement more precisely. Figure 6 displays the EBSD PAG reconstructions of the Study 2 dilatometry sample cross-sections. The starting PAG microstructure was similar to that shown in Figure 3(b), for the coarse columnar grained high interpass temperature build, as the samples were machined from the same wall. This microstructure was so distinctive and required such specific conditions to produce, that any finer equiaxed grain structures formed after thermal cycling in the dilatometer were assumed to be the result of grain refinement, the possible mechanism of which will be discussed later. Although the starting columnar PAG structure of the individual dilatometry

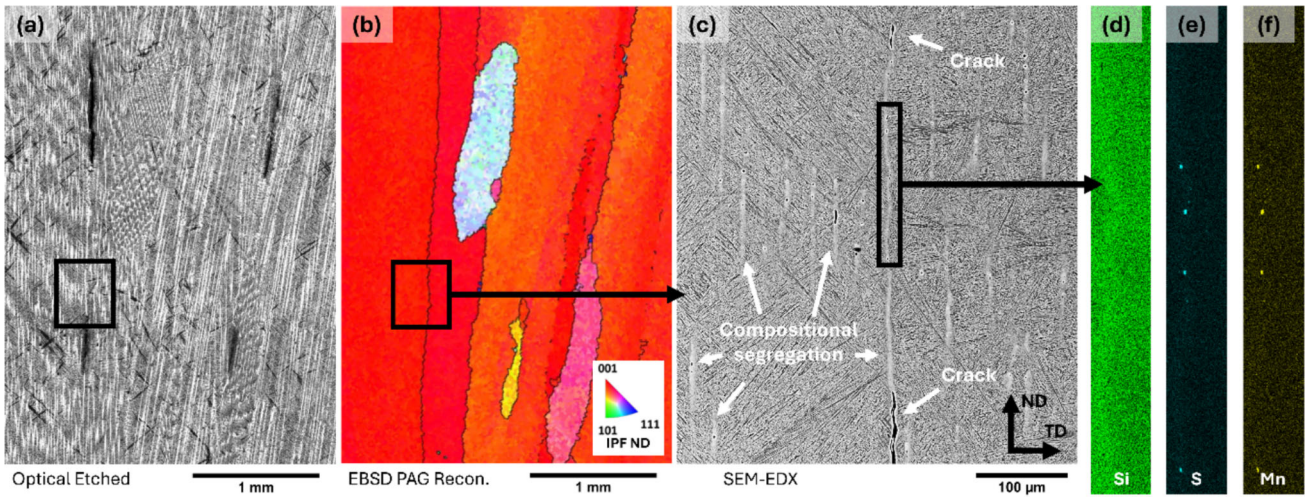


Fig. 5—(*a*) A magnified image of a cracked area from the Study 1 high interpass build optical map, also highlighted by an orange box in Fig. 3(b). (*b*) The EBSD PAG reconstruction from the same area with PAG boundaries in black (> 10 deg). The sample has been polishing back to an OPS finish in between optical and EBSD imaging, Cracks are not visible in the PAG reconstruction due to the coarse step size and cleaning steps performed to remove non-indexed pixels. (*c*) A BSE image of the region above one of the cracks in (a), (b), imaged after EBSD. (*d* to *f*) EDS K$\alpha$ intensity maps for Si, S and Mn from the region highlighted in (a), (b). Only Si is displayed in (d) to illustrate compositional microsegregation, other alloying elements segregate similarly.

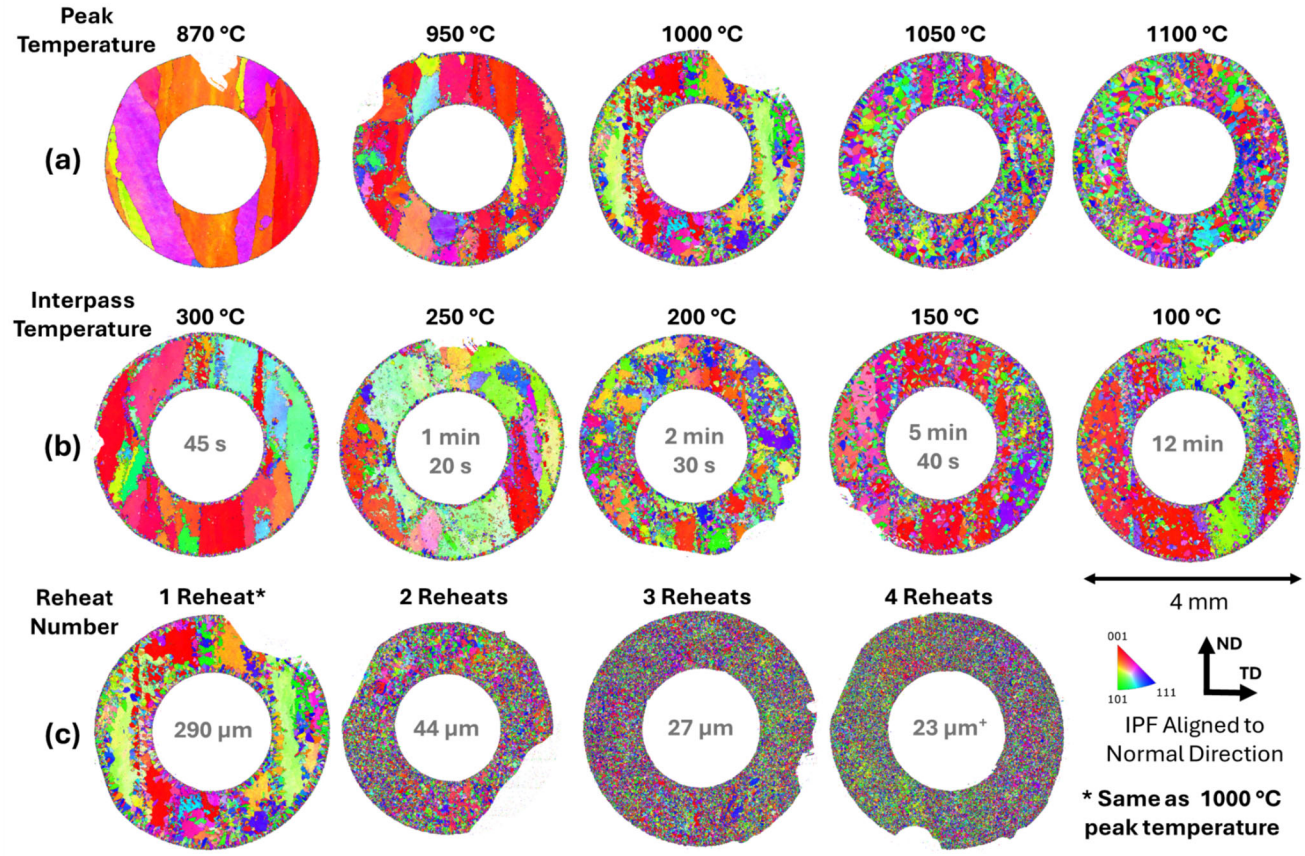


Fig. 6—EBSD montage maps of the Study 2 hollow dilatometry sample cross-sections after PAG reconstruction. The sections missing from the outer diameter of the rings are where silver paint was touched to the sample surface to prevent charging when using high beam current. (*a*) The peak temperature investigation samples. (*b*) The interpass temperature samples labelled with the time between passes in grey. (*c*) The number of heating cycle investigation samples. Equivalent circle diameter area weighted PAG size is labelled on each sample.

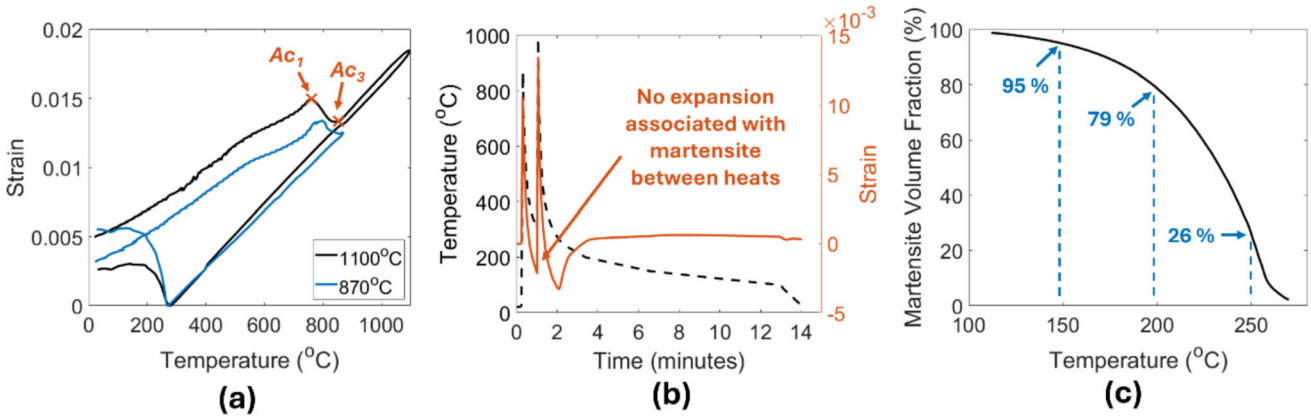


Fig. 7—(*a*) The dilatometry curve from the Study 2 870 °C and 1100 °C peak temperature test, the corresponding temperature profiles are shown in Fig. 2(a) and samples EBSD PAG reconstructions in Fig. 6(a). The 1100 °C sample can be seen to have fully austenitised on heating at 854 °C (before 870 °C). The heating segment of the curve is not straight before $Ac_1$ either due to the decomposition of retained austenite or the formation of carbides.[32] The data also contains some scatter due to the extreme 200 °C $s^{-1}$ heating rate used. (*b*) The temperature-time and strain-time profiles for the 300 °C interpass temperature test demonstrating that there was no expansion associated with the martensitic transformation between heats (only thermal expansion). This demonstrates there was no martensitic transformation between heats. (*c*) The volume fraction of martensite formed during cooling in the extra 100°$Cs^{-1}$ heating and cooling rate tests, calculated using the method in.[27,28] For this sample the Ms and Mf calculated using the offset method,[26] were measured at 270 °C and 112 °C, respectively.

samples varied from sample to sample, the PAG reconstruction of the high interpass temperature build in Figure 3(b) illustrates how the PAGs anywhere in this sample are often coarser than those found at the top of the low interpass temperature or CWMIG builds displayed later. Thus, the dilatometry samples were representative of a worst-case scenario for coarse grains in found at the top of a build, before reheating during subsequent passes.

Study 2 began by finding the peak temperature required for refinement during a rapid WAAM thermal cycle. It can be seen from Figure 6(a) that setting the peak temperature to that of the conventional austenitisation heat treatment temperature of 870 °C had no effect on the prior austenite grain structure, which was apparently reproduced on reheating above $A_{c3}$ by a memory effect (as discussed later). The dilatometry curves for the Study 2 870 °C and 1100 °C peak temperature samples are displayed in Figure 7(a). The 1100 °C peak temperature curve demonstrates that at this high heating rate the material was only just fully austenitised by 870 °C. This was also confirmed by measuring the austenite start and finish temperatures ($Ac_1$ and $Ac_3$) for this temperature profile using the 1 pct offset method[26] – an average of the 1000 °C, 1050 °C and 1100 °C peak temperature tests recorded $Ac_1$ as 765 °C and $Ac_3$ 859 °C, respectively. Both curves in Figure 7(a) demonstrate that the samples formed only martensite upon cooling.

Increasing the peak temperature across Figure 6(a), 950 °C led to the first emergence of refined austenite grains decorating the large columnar PAG boundaries. However, large columnar austenite grains still constituted a significant fraction of the overall microstructure until the peak temperature was raised above 1000 °C, where further increases of the peak temperature resulted in complete refinement of the microstructure by 1050 °C.

The second stage of Study 2 involved finding the maximum interpass temperature required for refinement. Dilatometry sample EBSD PAG reconstructions from these interpass temperature tests are shown in Figure 6(b). The times between passes that were needed to allow for cooling are displayed on the maps. An interpass temperature of 300 °C resulted in minimal grain refinement, despite a 1000 °C peak temperature [which Figure 6(a) demonstrated could produce refinement if the steel were allowed to cool to room temperature]. Refined austenite grains were observed decorating some but not all columnar PAG boundaries. Reducing the interpass temperature to 250 °C resulted in more non-memory grains distributed throughout the sample, and further reduction below 200 °C produced a significant grain refinement. The accompanying dilatometry curves in Figure 7(b) demonstrate that the 300 °C interpass sample did not form martensite before it was reheated, whilst the samples cooled to 250 °C and below did. In Figure 7(c) the approximate volume fractions of martensite formed upon cooling below $M_s$ were calculated using the 100 °C $s^{-1}$ constant heating and cooling rate dilatometry curve (non-WAAM temperature profile), using the method in reference.[27,28] From this, it was estimated that 26, 79 and 95 pct martensite formed in-between heats for the 250 °C, 200 °C and 150 °C simulated interpass temperature profiles, respectively. These values are not completely accurate, since they were calculated based on the assumption that 1 pct volume fraction of austenite remained at $M_f$, which was likely an underestimate, and the effects of residual stresses or the change in $M_s$ temperature with PAG size, which were ignored[29–31] ($M_s$ was 270 °C here but varied from 266 °C to 284 °C between the dilatometry tests investigating peak temperature). However, the results illustrate that there is a large difference in the transformed fraction between

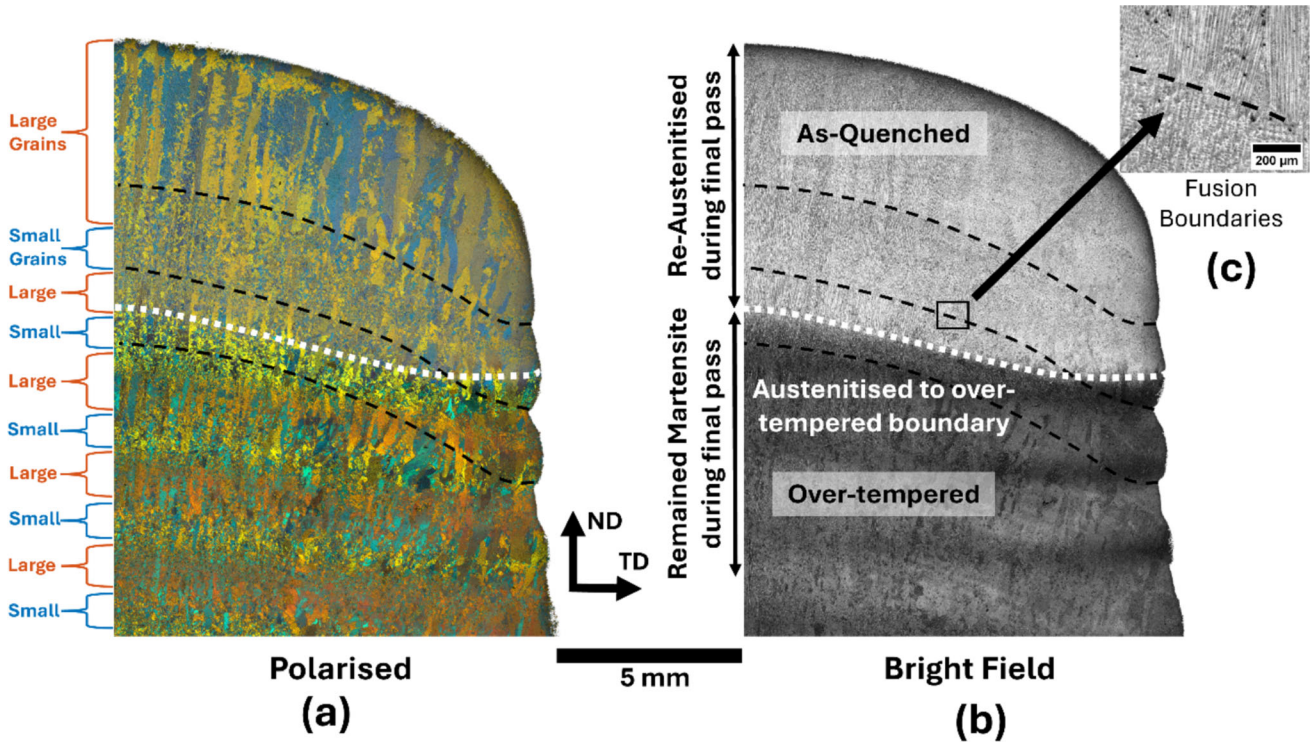


Fig. 8—(*a*), (*b*) Optical maps showing the top left corner of the Study 3 CWMIG build cross-section after etching in 2 pct nital. Polarized light was used to image (a) and regions of large and small PAGs are marked to the left of the image. Normal bright field was used to image (b), the material re-austenitised during the final pass appears light etching, whilst the material that remained martensitic was over-tempered and appears dark etching. The boundary between light and dark etching has been marked on both (a) and (b) with a white dashed line. A region of interest has been magnified in (*c*) to demonstrate how fusion boundaries can be recognized by a break in the interdendritic compositional microsegregation pattern highlighted by etching. The fusion boundaries from the final three passes were identified using (b) and have been marked onto both (a) and (b) using black dashed lines.

250 °C and 200 °C, and a very small difference below 200 °C.

The third and final aspect of Study 2 was to investigate the influence of thermal cycling at 1000°C on grain refinement. Figure 6(c) demonstrates how austenite grain size was reduced through multiple 1000 °C heating cycles, though with diminishing returns after each cycle. The area weighted equivalent circle diameter PAG sizes for each reheat are also displayed in Figure 6(c). After three reheating cycles the average PAG diameter of 27 $\mu$m (grain size No. 8.6 ASTM E2627) was comparable to that measured from a typical forged service component of 29 $\mu$m using the same EBSD parameters, and to the 25 $\mu$m measured from the Study 1 low interpass build. It was also well below the grain size required by the ASTM E112 standard for forged 300M aerospace parts (grain size No. 6 or finer).

### C. *Study 3: Assessing the Effect of HAZ Depth on the Homogeneity of PAG Refinement*

As described in the previous section, HAZ depth is important as it controls the number of layers that are thermally cycled to above 1000°C when depositing subsequent layers. Study 3 aimed to demonstrate the effect of varying HAZ depth. Figures 8(a), (b) display a polarized light map and bright field optical map from the same top corner of the CWMIG build cross-section – only a corner of the entire map is displayed to magnify microstructural features on the page. The polarized light map in Figure 8(a) reveals regions containing large columnar PAGs clearly, without the interference from the interdendritic microsegregation patterns or darkening due to tempering as seen in the corresponding bright field map. Polarized light reveals the PAGs because the light is scattered by carbides in martensite which protrude from the surface after etching. The carbides will have formed with specific orientation relationship (OR) to the martensite, which in turn has an OR with the PAG it formed from. Thus, each PAG, or at least packet will have scattered polarized light differently.[33] With the CWMIG wall the polarized map displayed a repeating pattern of layers of columnar PAGs and fine-grained regions. To compliment this, the bright field map in Figure 8(b) was able to show the depth of the region that was re-austenitised by the last pass as it appeared lighter etching (since the martensite was not tempered by subsequent passes). The boundary between the material that was re-austenitised and that which remained martensite is marked by a white dotted line in both maps, this boundary can be correlated approximately to where the material was heated to the $Ac_1$ temperature (765 °C) during the final pass. The optical map was also able to reveal the dendritic microsegregation structure formed during melt pool solidification, as most alloying elements in 300M segregate to the

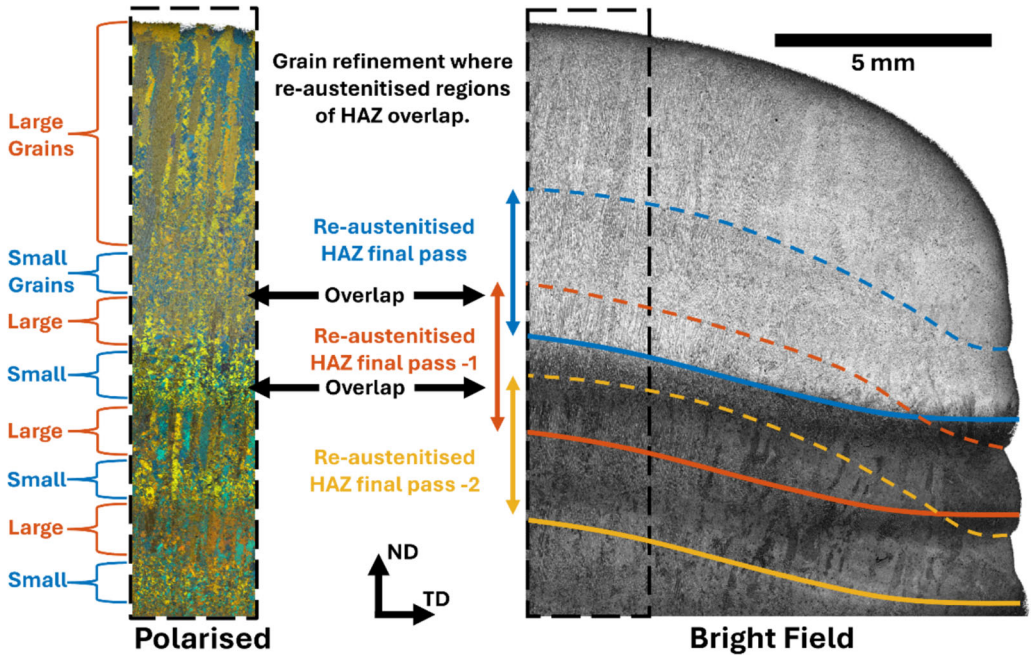


Fig. 9—The polarized and bright field optical maps from Study 3 CWMIG build also shown in Fig. 8. Here, the polarized light map has been cropped to more easily compare spatially aligned features between the two maps. Using the microstructural markers shown in Fig. 8 the fusion boundaries for the final three passes have been marked out with dashed lines, and the boundary above which the material was fully re-austenitised during the pass was marked with a solid lines (above $Ac_3$ 859 °C). As only the re-austenitised boundary for the final pass could be measured, the boundaries for the other passes were drawn assuming the same depth of re-austenitisation from the fusion boundary. Fusion boundaries and their corresponding re-austenitised boundaries are colour codes blue, orange and red according to the pass counting from the final pass. The region between the dashed and solid lines of the same colour must therefore be the material re-austenitised during that pass. It can be seen that the layers of small PAGs in the polarized light map, correspond to the regions with the top of the overlap between the re-austenitised regions of subsequent passes.

interdendritic regions (including Cr) causing them to etch lighter. It is important to note that the segregation pattern is related to solidification only, it does not necessarily relate to PAG boundaries or the present underlying microstructure (which also etches in nital), as these may undergo further changes after solidification or during reheating by subsequent passes. Figure 8(c) demonstrates how the fusion boundaries between layers could be identified by a break in the dendrite structure. This same microstructural feature could be identified in both the lighter and darker etching regions of the build, allowing the approximate depths of the material re-melted (or deposited) during the final 3 passes to be traced onto Figures 8(a) and (b) with black dashed lines. Note that all the lines marked on Figure 8 using microstructural features were drawn based on the use of a 150 °C interpass temperature and the reasonable assumption, supported by Figures 6(b) and 7, that the material transformed to martensite between passes. Interestingly, the re-austenitised region from the final pass (region above the white dotted line) overlaps approximately one and a half previously deposited layers, that is about two fusion boundaries.

Figure 9 displays a strip cropped from the left side of the polarized map in Figure 8(a) adjacent to the same section bright field map from Figure 8(b), allowing the repeating layers of large and small PAGs revealed by the polarized light to be aligned to microstructural structural boundaries revealed by the bright field. For clarity, the fusion boundaries from the last three passes are highlighted by dashed lines and the corresponding depth of re-austenitisation boundaries highlighted by solid lines. Since the depth of re-austenitisation boundary could only be identified for the final pass, the boundaries for the previous two passes have been drawn by assuming that the distance between the fusion boundary and re-austenitisation boundary was the same as for the final pass. The fusion and corresponding re-austenitised boundaries for each pass are colour coded blue, orange, and yellow, starting from the final pass. Thus, the depth of material re-austenitised by the HAZ during each respective pass is the material between dashed and solid lines of the same colour. Comparing the polarized map, with the re-austenitised regions reveals that the layers of small PAGs align with the top of the overlap between re-austenitised regions of subsequent passes. All the material in the build, barring the material deposited during the final pass, formed martensite and was re-austenitised once since the re-austenitisation depth is lower than the depth of the fusion boundary of the previous pass (*i.e.,* deeper than the depth of one layer). Where the re-austenitised regions overlap, the material was re-austenitised by the pass above it and again by the pass above that – in other words material here underwent two martensite to austenite and back to martensite cycles since deposition.

## IV. DISCUSSION

### A. *Role of Interpass Temperature*

Comparison of the Study 1 low and high interpass temperature builds [Figures 3(a), (b)] clearly demonstrates that a refined microstructure can be achieved in 300M WAAM by allowing the steel to cool to a temperature at which it can form martensite in between passes, regardless of the exact refinement mechanism. This means that the steel in the build was cycled between martensite and austenite during building. The top few layers of the build still contained large PAGs, but these only amount to a few millimetres that could be machined off from an industrial scale build.

In stark contrast, the high interpass build was likely austenitic until after the final layer was deposited. The light etching region covered most of the build [compare Figure 3(a) with (b)], and the transition from light to dark etching was less clearly defined (*i.e.,* the transition from as-quenched to over-tempered martensite). In addition, the thermocouple data in Figure 1(f) shows that the baseplate material did not fall below the $M_s$ temperature at all during building. Based on continuous-cooling transformation (CCT) data from the literature,[34] the presence of bainite in only the high interpass build (see Figure 4) indicates that this build was cooled much more slowly than its low interpass counterpart, likely due to heat build-up. Potentially, the bainite found at the base of the build [Figure 4(d)] formed during building whilst the sample temperature fluctuated between 300 °C and 600 °C for nearly 20 minutes [Figure 1(f)].

It is not entirely clear why cracks were found in the high interpass build after deposition. However, this detrimental behaviour, which would prevent the applicability of AM processing to high strength steels, is clearly linked to the coarse columnar grain structure that developed after solidification. Notably, cracks were not seen in the build produced with a refined austenite grain structure. Cracking is typically driven by residual stresses arising result from the large temperature gradient across the whole build during cooling. By comparison, the low interpass temperature build experienced steeper temperature gradients, but across smaller volumes of material near the top of the build where there is less constraint from surrounding material. In contrast, the high interpass build appears to have had a lower tolerance to residual stress accumulation, likely due to several microstructural factors. In particular, the presence of long, coarse columnar PAGs aligning in the high interpass temperature wall with compositionally enriched boundaries, where both alloy carbides, MnS particles and other impurities were concentrated (see Figure 5), would provide a weak site and path for crack initiation and propagation.[13,24,35,36] The effect of this poor microstructure may have also been exacerbated by the strong austenite texture, or residual stresses, influencing variant selection, as well as by the anisotropic volume change associated with the martensitic transformation.[37,38] The material deposited with the high interpass temperature would also be expected to have a poorer intrinsic fracture toughness, resulting from large PAG size and the corresponding larger martensite lath size.

Overall, the lack of cracking in the low interpass wall is most probably simply due to its greatly refined grain size. However, in this build, martensitic layers that were already refined through multiple austenitisation heat treatments were also then heavily tempered as more layers were added and they moved into the $< A_{c1}$ region of the HAZ. This is evident from the fact that all but the top of the low interpass temperature build etched darker [Figure 3(a)]. Reheating to just below $A_{c1}$ would have therefore enabled some degree of softening and the relaxation of residual stresses.

### B. *Mechanism of Austenitisation and Grain Refinement in 300M*

The phenomenon of PAG refinement by repeated austenitisation heat treatments in martensitic steels is well known,[7,24] but has not previously been investigated in the context of WAAM, where the moving heat source naturally results in a cyclic thermal history. The PAG refinement process has been shown to take place in two stages in some alloys,[39–50] including 300M.[9] The first stage is an austenite 'memory effect' whereby the morphology and crystallographic orientation of the PAGs are re-formed during re-austenitisation, albeit that the re-formed (memory) PAGs contain more internal misorientation and sub-structure than the original PAGs.[46–53] The second stage, which is not always observed, is where the steel undergoes recrystallisation without the application of external deformation during or after austenitisation (via the memory effect) has completed.[42–44,46,49,50]

Dilatometry experiments at heating rates up to 200 °C $s^{-1}$ showed a memory effect in martensite, as evidenced by the near full re-emergence of columnar austenite grains in the 870 °C single heat dilatometry sample [Figure 6(a)] from Study 2. The sample was austenitised during heating as demonstrated using dilatometry in Figure 7(a), whilst the distinctive columnar PAG structure can be safely assumed to have first been formed during WAAM. Previous work[9] has used in situ EBSD to demonstrate that a memory effect occurs in 300M even at very slow heating rates (33 °C per hour), meaning it is likely that a memory effect occurs at a wide variety of heating rates. It is therefore reasonable to assume that all the dilatometry samples initially underwent a memory effect during austenitisation, as all the samples were heated at the same heating rate through 870 °C before achieving higher peak temperatures. However, only those samples that were further heated beyond 1000-1050 °C began to recrystallize.

The mechanism of the PAG refinement observed could either have been the recrystallisation of memory austenite or the nucleation of new non-memory orientation austenite grains during the ferrite-austenite transformation. Here, it is most likely that recrystallisation was responsible for the grain refinement, because the PAG reconstruction of the 870 °C peak temperature sample [Figure 6(a)] displayed no evidence of the small,

refined grains that appear in the 950 °C peak temperature sample [also Figure 6(a)], which received an identical heat treatment but was heated further. As shown by the dilatometry in Figure 7(a) the ferrite-austenite transformation was fully completed by 870 °C, so any non-memory orientation austenite grains nucleated during austenitisation should already have been present.

In the authors' previous in situ EBSD reheating study,[9] 300M was found to recrystallize after austenitisation mainly through the bulging of high angle grain boundaries, and that this limited the extent of the recrystallisation that took place, since no new grains were nucleated. Indeed, it was observed that two neighbouring columnar grains would simply grow into one another, sweeping out the misorientation sub-structure (and presumed dislocation density) in their counterpart, which still led to a relatively coarse grain size. The far greater extent of refinement seen here in the samples rapidly heated to peak temperatures above 950 °C suggests that it is unlikely that boundary bulging was the only recrystallisation mechanism which occurred, as more grain nuclei would be required to explain the small grain size. The nucleation of new recrystallized grains was probably due to the greater heating rates and higher resulting driving forces (as recovery would be more limited) involved compared to the previously reported in situ work. Recrystallisation following the austenite memory effect has also been shown by several authors[39–42,49,54] to lead to a decreasing grain size with increasing heating rate in other steel alloys. Similar to their work, the non-memory orientation grains that we observe first concentrate on the grain boundaries of memory orientation austenite grains, before the memory austenite structure is then consumed by subsequent recrystallisation (see 950 °C and 1000 °C peak samples in Figure 6(a)].

It is worth noting that with WAAM reheating cycles, recrystallisation did not take place at the conventional 300M austenitisation heat treatment temperature of 870 °C. This is likely to be due to the rapid heating rates involved and lack of an isothermal hold at the peak temperature involved in the simulated thermal cycles used here. Even if there was sufficient driving force for recrystallisation, the hold time at temperature was insufficient for recrystallisation to complete or even start in the case of the 870 °C samples. For WAAM-based temperature profiles, higher temperatures must therefore be used to achieve recrystallisation than would be necessary for a slower heating rate conventional heat treatment. For this reason, the exact parameters found in this work should not be used for a conventional heat treatment.

### C. *Conditions for Building Refined 300M by WAAM*

Study 2 aimed to determine the minimum conditions needed for the production of WAAM builds with a refined PAG structure in 300M. Based on the EBSD PAG reconstructions in Figure 6(a), the minimum peak temperature that caused significant recrystallisation of the columnar PAGs, was found to be between 950 °C and 1000 °C assuming a heating rate similar to 200 °C $s^{-1}$ (as used here). During WAAM of 300M, it can therefore be considered that the entire HAZ from under the melt pool down to the depth that reached ~ 1000 °C undergoes recrystallisation, and that it does not below this temperature. Thus, this minimum peak temperature was then used for the interpass temperature and reheat number studies.

Regarding the interpass temperature requirement, although significant recrystallisation was seen in the dilatometry sample where a 200 °C interpass temperature was used [Figure 6(b)], an interpass temperature of 150 °C represents a safer case in this regard and should be used when building 300M. Dilatometry from Figure 7(c) demonstrates how a small increase in interpass temperature leads to a significant drop in martensite formation, which may significantly affect the extent of recrystallisation. This sensitivity was seen in the 250 °C sample where Figure 7(c) would suggest 26 pct martensite still formed, but recrystallisation was minimal. Since the interpass temperature internal to the wall cannot always be accurately measured, using 150 °C allows for a much larger margin of error, whilst requiring significantly less cooling time between passes than cooling to 100 °C [Figure 6(b)]. It is likely that the sensitivity of the recrystallisation of austenite during heating to the interpass temperature is derived from the fact that the austenite recrystallisation is driven by the deformation from the ferrite (martensite) to austenite transformation[44,46–50] (the details of which are not in scope here, but are being considered by the authors at present). If less martensite forms during cooling due to a higher interpass temperature, there is less martensite to transform to austenite during thermal cycling, resulting in less transformation strain to drive the recrystallisation of austenite (regardless of the exact mechanism by which it is generated). It is worth noting that the CWMIG build (Figure 8) contained at least some layers of grain refinement, unlike the Study 1 high interpass temperature build [Figure 3(b)]. This practically demonstrates that the 150 °C interpass temperature, suggested based on Study 2 and used for Study 3, was valid.

As shown in Figure 6(c), the austenite grain size significantly refined after two reheat thermal cycles above 1000 °C and was equivalent to that of conventionally manufactured material (~ 29 $\mu$m) after three cycles. During building, two reheat cycles above 1000°C would be achieved if the depth of re-austenitisation to 1000 °C below the fusion boundary overlapped two previously deposited layers into the material. This was practically demonstrated by the Study 3 CMWP build in Figure 9, where the depth of re-austenitisation covered approximately one and a half previously deposited layers, or two fusion boundaries. All the material was re-austenitised once, but only half of each layer was cycled between martensite and austenite a second time to produce any significant grain refinement. The result was sections of material that miss out on grain refinement altogether, and corresponding alternating layers of coarse and fine PAGs. By comparison, the depth of material re-austenitised in the Study 1 low interpass temperature build [see light etching region of

Figure 3(a)] covered multiple layers, although it was difficult to count exactly how many due to some slight wavering in the torch path causing fusion boundaries to meld into each other (between 3 and 5 fusion boundaries within the light etching region). This resulted in all but the final three layers of material being cycled above 1000 °C at least three times, producing a very fine PAG structure.

For building real parts, it can be considered that only a minimum of two reheats (not three) would be necessary to achieve a PAG size comparable to that of a conventionally forged component. This is because the as-built material in a WAAM'd 300M wall is typically in an over-tempered state (see the dark etching regions of the etched samples in Figures 3 and 8) and would require a conventional single austenitisation, quench and temper treatment before service (the same as any forged component). As such, the build would receive a third reheat to austenitisation treatment anyway. Of course, this would be below 1000°C (e.g., at 870°C), but the longer hold times involved should allow time for recrystallisation.[7,11] During building, two reheats are sufficient to break up the columnar austenite grain structure of previous layers [see Figure 6(c)] and thus prevent cracking associated with large highly textured grains.

### D. *Rules for 300M WAAM, and Extension to Other Martensitic Steels*

In summary, there are two main rules that should be followed to successfully build 300M components using WAAM:

- A low interpass temperature must be used to enable the martensitic transformation to take place before the next pass is deposited. As a guide, for 300M, the local material temperature should therefore be allowed to fall to ~ 150 °C before the heat source returns. This is illustrated schematically in Figure 10(a).
- The depth of material reheated above the temperature-profile-dependent effective recrystallisation temperature (~1000 °C), measured from below the fusion boundary, should ideally be greater than the depth of the two previously deposited layers measured by their fusion boundaries (excluding the final layer deposited). This is illustrated schematically in Figure 10(b).

Theoretically, these rules should apply across different WAAM processes for 300M regardless of processing variables such as the heat source. Indeed, the general premise of the rules should apply to any ferritic steel that austenitises with a memory effect and then recrystallizes at the heating rates found in WAAM. However, it is likely that the temperature to which the material must be reheated in the HAZ will change from alloy to alloy, as could the number of reheating cycles required. This could add a new dimension to alloy selection for WAAM. For example, steels with $M_s$ temperatures below 100 °C may be impractical to manufacture with a low enough interpass temperature, meaning other routes must be used to achieve a fine grain size. It is also equally important to consider the temperature at which recrystallisation effectively starts in the alloy, given the short time at high temperature. This could be affected by factors such as grain boundary pinning particles, or even whether memory effect austenitisation and recrystallisation occur simultaneously or at different temperatures.

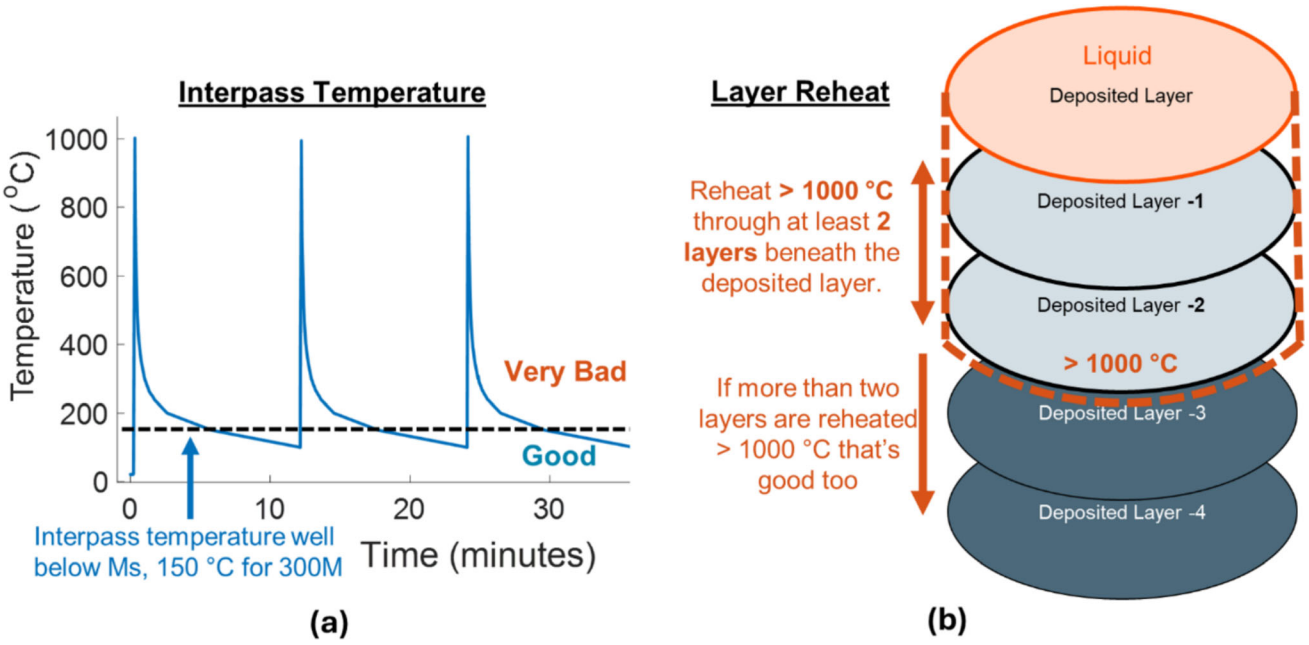


Fig. 10—A schematic showing the rules for achieving PAG refinement in 300M or similar steels during WAAM: (*a*) low interpass temperature and (*b*) sufficient HAZ overlap to reheat previously deposited layers.

## V. CONCLUSION

This work has demonstrated that a fine PAG size comparable to that of a conventionally manufactured forged component may be produced in as-built WAAM 300M, by exploiting recrystallisation associated with cyclic, rapid re-austenitisation. This was achieved in practice using a low interpass temperature and a large HAZ overlap, such that the steel was repeatedly cycled between austenite and martensite during building.

Ex situ heat treatments in a dilatometer and subsequent EBSD of the samples revealed that, under rapid heating conditions (~ 200 °C $s^{-1}$), from a martensitic structure 300M undergoes austenitisation with a memory effect followed by recrystallisation without the application of external deformation, which leads to a fine austenite grain size and weak texture.

The specific conditions needed for successful PAG refinement in 300M WAAM were determined using the dilatometry experiments. Two rules that must be implemented in order to achieve grain refinement during WAAM of 300M are proposed as follows:

- A low interpass temperature should be used, so that the material is cooled to well below the material's martensite start temperature (150 °C is suggested for 300M).
- The region of the HAZ exceeding the temperature at which recrystallisation occurs, must overlap more than two previously deposited layers. This temperature (of around 1000°C for 300M) is expected to be significantly higher than the temperature at which recrystallisation occurs during a conventional heat treatment due to the minimal time available for recrystallisation, resulting from the rapid thermal cycle experienced with WAAM temperature profiles.

It was suggested that these rules should be transferable to ferritic steels with similar phase transformation behaviour to 300M, though the specific temperature parameters may change.

The rules were validated in practice through the characterization of a WAAM'd 300M wall with different HAZ depths relative to the layer height deposited. This highlighted the importance of maintaining a sufficient HAZ overlap for achieving consistent grain refinement.

## ACKNOWLEDGMENTS

This work was undertaken within the ATI I-Break project led by Airbus. I-Break is a collaborative research project involving multiple UK partners to develop alternatives to forging manufacturing technology for landing gear applications. The authors gratefully acknowledge financial support from Innovate UK (project reference 10003486). The authors acknowledge the use of equipment associated with the Advanced Metals Processing and Characterisation themes of the Henry Royce Institute for Advanced Materials, funded through EPSRC grants EP/R00661X/1, EP/S019367/1, EP/P025021/1 and EP/P025498/1. Many thanks to Richard Wood and Ian Brooks at Additure for building the CWMIG WAAM component. The raw data associated with this manuscript can be found here: https://doi.org/10.5281/zenodo.17106852

## CONFLICT OF INTEREST

The authors declare that they have no known competing financial interests or personal relationships that could have appeared to influence the work reported in this paper.

## OPEN ACCESS

This article is licensed under a Creative Commons Attribution 4.0 International License, which permits use, sharing, adaptation, distribution and reproduction in any medium or format, as long as you give appropriate credit to the original author(s) and the source, provide a link to the Creative Commons licence, and indicate if changes were made. The images or other third party material in this article are included in the article's Creative Commons licence, unless indicated otherwise in a credit line to the material. If material is not included in the article's Creative Commons licence and your intended use is not permitted by statutory regulation or exceeds the permitted use, you will need to obtain permission directly from the copyright holder. To view a copy of this licence, visit http://creativecommons.org/licenses/by/4.0/.

## REFERENCES

1. S.W. Williams, F. Martina, A.C. Addison, J. Ding, G. Pardal, and P. Colegrove: *Mater. Sci. Technol.*, 2016, vol. 32, pp. 641–47.
2. F. Martina, J. Mehnen, S.W. Williams, P. Colegrove, and F. Wang: *J. Mater. Process. Technol.*, 2012, vol. 212, pp. 1377–86.
3. W. Ou, T. Mukherjee, G.L. Knapp, Y. Wei, and T. DebRoy: *Int. J. Heat Mass Transf.*, 2018, vol. 127, pp. 1084–94.
4. J. Wang, C. Diao, M. Taylor, C. Wang, E. Pickering, J. Ding, M. Pimentel, and S. Williams: *Int. J. Adv. Manuf. Technol.*, 2023, vol. 129, pp. 3751–67.
5. T.A. Rodrigues, V.R. Duarte, D. Tomás, J.A. Avila, J.D. Escobar, E. Rossinyol, N. Schell, T.G. Santos, and J.P. Oliveira: *Addit. Manuf.*, 2020, vol. 34, 101200.
6. Y. Xu, B. Mishra, and S.P. Narra: *Mater. Charact.*, 2022, vol. 190, 112065.
7. Y. Tomita and K. Okabayashi: *Metall. Trans. A*, 1985, vol. 16, pp. 83–91.
8. R.A. Grange and E.R. Shackelford: *Method of Producing Ultrafine Grained Steel*, U.S. Pat. 3,178,324, 1965, assigned to U.S. Steel Corp.
9. M. Taylor, Y.H. Mozumder, A.D. Smith, A.E. Davis, F. Scenini, P.B. Prangnell, and E.J. Pickering: *IOP Conf. Ser.*, 2024, vol. 1310, p. 012001.
10. G. Zhang, X. Yang, X. He, J. Li, and H. Hu: *Mater. Des.*, 2013, vol. 45, pp. 56–66.
11. L. Youngblood and Raghavan, M: *Microstructure and Mechanical Properties of Quenched and Tempered 300M Steel*, No. NASA-TP-1288, 1978.
12. W.-D. Cao and X.-P. Lu: *Metall. Trans. A*, 1987, vol. 18, pp. 1569–85.

13. Y. Tomita: *Mater. Sci. Technol.*, 1991, vol. 7, pp. 97–104.
14. T. Skiba, B. Baufeld, and O. Van der Biest: *Proc. Inst. Mech. Eng. Part B*, 2011, vol. 225, pp. 831–39.
15. Y. Xiong, D. Wen, Z. Zheng, and J. Li: *Mater. Sci. Eng. A*, 2022, vol. 831, 142351.
16. Y. Xiong, D. Wen, Z. Zheng, C. Sun, J. Xie, and J. Li: *Mater. Charact.*, 2023, vol. 198, 112756.
17. F. Liu, X. Lin, J. Shi, Y. Zhang, P. Bian, X. Li, and Y. Hu: *Addit. Manuf.*, 2019, vol. 29, 100795.
18. G. Jing and Z. Wang: *J. Mater. Process. Technol.*, 2021, vol. 296, 117188.
19. J.D. Verhoeven: *J. Mater. Eng. Perform.*, 2000, vol. 9, pp. 286–96.
20. G. Krauss: *Metall. Mater. Trans. B*, 2003, vol. 34B, pp. 781–92.
21. X. He, X. Yang, G. Zhang, J. Li, and H. Hu: *Mater. Des.*, 2012, vol. 40, pp. 386–91.
22. F. Liu, X. Lin, M. Song, H. Yang, Y. Zhang, L. Wang, and W. Huang: *J. Alloy Compd.*, 2015, vol. 621, pp. 35–41.
23. R.A. Rahman Rashid, C.J. Barr, S. Palanisamy, K.A. Nazari, N. Orchowski, N. Matthews, and M.S. Dargusch: *Surface and Coatings Technology*, 2019, vol. 380, p. 125090.
24. Y. Tomita: *Mater. Sci. Technol.*, 1991, vol. 7, pp. 481–89.
25. M. Pan, J. Xu, N. Liang, Y. Peng, Q. Zhou, and K. Wang: *Mater. Sci. Eng. A*, 2023, vol. 881, 145300.
26. H.-S. Yang and H.K.D.H. Bhadeshia: *Mater. Sci. Technol.*, 2007, vol. 23, pp. 556–60.
27. S.J. Lee, J.S. Park, and Y.K. Lee: *Scripta Mater.*, 2008, vol. 59, pp. 87–90.
28. S.M.C. Van Bohemen and J. Sietsma: *Mater. Sci. Technol. (United Kingdom)*, 2014, vol. 30, pp. 1024–33.
29. H.S. Yang and H.K.D.H. Bhadeshia: *Scr. Mater.*, 2009, vol. 60, pp. 493–95.
30. C. Celada-Casero, J. Sietsma, and M.J. Santofimia: *Mater. Des.*, 2019, vol. 167, 107625.
31. M. Taylor, J.W. Fellowes, P.O. Hill, M.J. Rawson, T.L. Burnett, and E.J. Pickering: *IOP Conf. Ser. Mater. Sci. Eng.*, 2022, vol. 1249, p. 012061.
32. W. Zheng, J. Zhu, and W. Yuan: *Mater. Charact.*, 2023, vol. 197, 112688.
33. S. Reisinger, G. Ressel, S. Eck, and S. Marsoner: *Micron*, 2017, vol. 99, pp. 67–73.
34. R. Chen, Z. Zheng, N. Li, J. Li, and F. Feng: *Mater. Charact.*, 2018, vol. 144, pp. 400–10.
35. G.Y. Lai, W.E. Wood, R.A. Clark, V.F. Zackay, and E.R. Parker: *Metall. Trans.*, 1974, vol. 5, pp. 1663–70.
36. C.L. Briant: *Mater. Sci. Technol.*, 1989, vol. 5, pp. 138–47.
37. Y. Matsuoka, T. Iwasaki, N. Nakada, T. Tsuchiyama, and S. Takaki: *ISIJ Int.*, 2013, vol. 53, pp. 1224–30.
38. F. Archie, M.Z. Mughal, M. Sebastiani, E. Bemporad, and S. Zaefferer: *Acta Mater.*, 2018, vol. 150, pp. 327–38.
39. S. Matsuda and Y. Okamura: *ISIJ Int.*, 1974, vol. 14, pp. 363–68.
40. S. Matsuda and Y. Okamura: *ISIJ Int.*, 1974, vol. 14, pp. 444–49.
41. S.T. Kimmins and D.J. Gooch: *Met. Sci.*, 1983, vol. 17, pp. 519–32.
42. S.S. D'yachenko: *Met. Sci. Heat Treat.*, 2000, vol. 42, pp. 122–27.
43. T. Hara, N. Maruyama, Y. Shinohara, H. Asahi, G. Shigesato, M. Sugiyama, and T. Koseki: *ISIJ Int.*, 2009, vol. 49, pp. 1792–1800.
44. L. Liu, Z.-G. Yang, C. Zhang, and W.-B. Liu: *Mater. Sci. Eng. A*, 2010, vol. 527, pp. 7204–09.
45. L. Liu, Z.-G. Yang, and C. Zhang: *J. Alloy Compd.*, 2013, vol. 577, pp. S654-660.
46. T. Shinozaki, Y. Tomota, T. Fukino, and T. Suzuki: *ISIJ Int.*, 2017, vol. 57, pp. 533–39.
47. Y. Tomota, W. Gong, S. Harjo, and T. Shinozaki: *Scripta Mater.*, 2017, vol. 133, pp. 79–82.
48. H. Shirazi, G. Miyamoto, S. Hossein Nedjad, T. Chiba, M. Nili Ahmadabadi, and T. Furuhara: *Acta Mater.*, 2018, vol. 144, pp. 269–80.
49. G. Ressel, D. Brandl, T. Hönigmann, M. Lukas, A. Stark, C. Gruber, S. Lukas, M. Stockinger, and E. Kozeschnik: *Mater. Des.*, 2023, vol. 234, 112370.
50. A. Rosenauer, D. Brandl, G. Ressel, T. Hönigmann, M. Stadler, C. Turk, C. Gammer, M. Wiessner, E. Gamsjäger, M. Stockinger, and R. Schnitzer: *Mater. Charact.*, 2024, vol. 208, 113554.
51. D. Brandl, M. Lukas, M. Stockinger, S. Ploberger, and G. Ressel: *Mater. Des.*, 2019, vol. 176, 107841.
52. A. Rosenauer, D. Brandl, G. Ressel, S. Lukas, C. Gruber, M. Stockinger, and R. Schnitzer: *Adv. Eng. Mater.*, 2023, vol. 25, p. 2300410.
53. N. Nakada, R. Fukagawa, T. Tsuchiyama, S. Takaki, D. Ponge, and D. Raabe: *ISIJ Int.*, 2013, vol. 53, pp. 1286–88.
54. X. Zhang, G. Miyamoto, Y. Toji, S. Nambu, T. Koseki, and T. Furuhara: *Acta Mater.*, 2018, vol. 144, pp. 601–12.

**Publisher's Note** Springer Nature remains neutral with regard to jurisdictional claims in published maps and institutional affiliations.

https://dspace.org/

# Microstructure engineering during wire-arc additive manufacturing of high-strength martensitic steels

**Taylor, Mark; Wang, Jun; Mozumder, Yahya H.; Williams, Stewart W.; Scenini, Fabio ...**

**2025-12**
Springer
https://doi.org/10.1007/s11661-025-07988-x
Taylor M, Wang J, Mozumder YH, et al., (2025) Microstructure engineering during wire-arc additive manufacturing of high-strength martensitic steels. Metallurgical and Materials Transactions A, Volume 56, December 2025, pp. 5521-5536

Downloaded from a DSpace repository. https://dspace.org/